Preprint version
Final version of this paper is published as: Flessa, Aikaterini, et al. “Raman Mapping of 4-MeV C and Si Channeling Implantation of 6H-SiC.” Journal of Raman Spectroscopy, vol. 50, no. 8, Aug. 2019, pp. 1186–96. DOI.org (Crossref), doi:10.1002/jrs.5629.

Raman mapping of C and Si channeling implantation of SiC

A. Flessa, E. Ntemou, M. Kokkoris, E. Liarokapis*

Department of Physics, National Technical University of Athens, Zografos GR-15780, Greece

M. Gloginjić, S. Petrović, M. Erich

Laboratory of Physics, Vinča Institute of Nuclear Science, University of Belgrade, P.O.Box 522, 11001 Belgrade, Serbia

S. Fazinić, M. Karlušić, K. Tomić

Laboratory for Ion Beam Interactions, Department of Experimental Physics, Institut Ruđer Bošković, Bijenička cesta 54, 10000 Zagreb Croatia

**email: eliaro@central.ntua.gr*

ABSTRACT

A 6H-SiC single crystal irradiated in channeling mode by 4 MeV C^{+3} and Si^{+3} ions at various doping levels have been examined by SEM and micro-Raman spectroscopy in order to study the lattice distortions inflicted by the impinging ions. C ions create zones of strongly damaged regions, parallel to the front face of the wafer with width increasing with the amount of doping. As expected, Si has induced considerably more lattice distortions than C and almost two orders of magnitude less doping induces apparently the same effect as C. Despite the large laser spot size compared with the boundaries of the distorted regions, micro-Raman data provided results agreeing with the SEM pictures and the Monte Carlo calculations using the SRIM-2013 software. From the evolution of the crystalline peaks in the Raman spectra one can conclude that the impinging ions do not accommodate as defects in the lattice, but mostly displace the ions breaking the bonds and destroying the long range order.

INTRODUCTION

Silicon Carbide (SiC) is a wide band-gap semiconductor and has attracted an increasing attention during the recent years, due to its exceptional physical properties (extreme hardness, high-temperature strength, chemical inertness and low-thermal expansion) that render it as a promising substitute for traditional semiconductors. These properties make it suitable for the development of high-temperature, high-power and high-frequency electronic devices [1, 2].

In the past years, extensive studies have been carried out regarding the irradiation effects in SiC induced by heavy-ions or neutrons at different temperatures and concerning the microstructure, amorphization, annealing processes, and recrystallization of the SiC [3, 4]. High-energy ion implantation (MeV energy range) is considered to be a promising technique for designing multi-layer, three-dimensional structures deep inside the crystalline material and subsequently increasing the microelectronic chip integration. Moreover, by orienting the ion beam along a crystallographic axis (channeling mode), a deeper implantation in the crystal is expected as a consequence, in comparison with the 'random' ion beam solid orientation, as well as a minimization of the induced lattice crystal damage [5].

A detailed investigation of the way carbon and silicon ions are implanted is of fundamental interest for potential device applications, principally for carbon, which is a well known contaminant in transistors and diodes and, when implanted in high doses, modifies their mechanical and electrical properties [6]. However, there is a certain lack in literature concerning data in the case of high-energy ion implantations in the channeling orientation, especially concerning high-dose, high-energy channeling implantation of carbon and silicon ions in SiC. Xiaofei Chen et al. have studied the irradiation effects in 6H-SiC induced by high- dose, high-energy carbon and silicon ions, but only in the 'random' orientation and with limited information from the Raman investigation [4].

The majority of the radiation damage and annealing studies of SiC have employed either ion-channeling methods based on Rutherford or elastic backscattering spectrometry (RBS-EBS/C) or TEM (Transmission Electron Microscopy) [7-10]. In this paper, micro-Raman spectroscopy has been used to provide detailed information about the in-depth distribution of effects induced by high-energy ion beams [3, 5, 11] in connection with SEM (Scanning Electron Microscopy) characterization. The lattice disorder and strain of 6H-SiC implanted

with 4 MeV carbon and silicon ions, was studied at various doses in the channeling orientation. Raman line intensities, shifts and bandwidths have been used to investigate the defects in the ion implanted regions. Raman spectroscopy as an optical method has the advantage of being a non-contact analysis tool that requires little or no sample preparation. Also, Raman scattering efficiency of SiC is relatively high due to the strong covalency of the chemical bonds [12]. Raman spectra can provide information about the polytype of SiC, the disorder or damage, impurities, lattice strain, free carrier density and mobility, as well as details about the composition and the chemical structure of the damaged layers [3, 13-18]. In this work we will concentrate on the Raman study of the distribution of damage induced by the ion irradiation.

EXPERIMENTAL DETAILS

N-type, 6H-SiC single crystal wafers of 330 μm thickness and (0001) orientation, were used in this work. The channeling and random ion implantations were carried out at Ruđer Bošković Institute, Croatia, using the 1 MV Tandetron accelerator. The effect of ion implantation was studied by 4 MeV C^{+3} and Si^{+3} ions and the ion fluence ranged from $4.17x10^{14}$ to $2.02x10^{16}$ particles/cm^2. As listed in Table I, all spots were the result of channeling irradiation except one (spot 7), which was obtained with the beam deviating from channeling mode. The ion irradiated spots had a size of 1x1 mm^2 and the beam current did not exceed 8 nA on target. Protons at 1, 1.725, and 1.86 MeV were used to align the beam to the (0001) axis of the crystal and for subsequent EBS/C studies.

The micro-Raman and SEM measurements were performed on the side surfaces of the transversally cleaved wafers. For the Raman measurements a Jobin-Yvon T64000 triple spectrometer with liquid nitrogen cooled CCD was used for data collection. To avoid local heating from the 514.5 nm line of an Ar+ laser, the power on the sample was kept below 0.6 mW. By employing a 100 objective lens in the microscope, the size of the laser beam spot was ~1 μm and the mapping of the damaged area was performed with a step of 0.2 μm of the micro-positioner. The Raman bands were fitted with multiple Lorentzian and Gaussian bands including a polynomial background. For the SEM pictures, a Nova NanoSEM 230 instrument has been employed.

RESULTS AND DISCUSSION

The SEM image shown in Fig.1a corresponds to the C^{+3} ion implantation with ion fluence $1.35x10^{15}$ ions/cm^2 (spot 4) and presents the characteristic modifications induced by the ion irradiation inside the SiC wafer. Similar effects have been found for the other C doses and indicate that there are strongly distorted regions from the heavy ion implantation, which appear as zones parallel to the surface and their location and width depends on the ion and the dose. The boundary of the zone closer to the front surface seems wider compared to the other one that looks more abrupt. Fig.1b presents the corresponding effects from the low dose Si^{+3} implantation in which case the lattice distorted regions are located roughly ~1-2 μm from the surface, i.e., closer to the surface than for the C implantations (roughly ~2-3 μm from the surface). For the high Si doses the distortions are so strong that the boundary of the damaged zone is not well defined. The other narrow zones that appear deeper inside the wafer for both C and Si irradiation are due to protons of varying energies used to align the beam with the (0001) axis and for the EBS/C analysis. From all SEM images it was found that the distribution of the ions was parallel to the surface of the wafer and the damaged regions in the whole area of the irradiated spot were homogeneous and dropped abruptly at their edges. These findings will be compared below with the results of micro-Raman mapping of the damaged regions. It should be noted that due to the size of the laser beam spot, the detected spectra correspond to a convolution from areas of ~1 μm diameter, as measured by scanning the laser beam across the side surface of the virgin SiC (inset in Fig.2).

The phonons of 6H-SiC are divided into planar and axial modes according to the orientation of the atoms, perpendicular or parallel to the c-axis, respectively [19]. The folded modes of crystalline 6H-SiC correspond to phonons with a wave vector of $q=2\pi m/(nc)$ in the basic Brillouin zone of the 3C-polytype in the [111] direction, where n=6 the number of formula units (Si-C) in the unit cell, m is an integer ($2m \leq n$) and c is the unit cell length.[17, 19] The Raman active phonon modes of 6H-SiC are of A_1, E_1 and E_2 symmetry, where A_1 and E_1 modes are split into longitudinal (LO) and transversal (TO) optical modes [19]. The peaks detected from the non-irradiated wafer (bottom spectrum of Fig.2) are consistent with the 6H-SiC structure and are located at ~149, 240, 265, 507, 515, 770, 791 and 800 cm^{-1}, corresponding to E_2-FTA (2/6) (Folded Transversal Acoustic mode), E_1-FTA (4/6), E_2-FTA (6/6), A_1-FLA (4/6) (Folded Longitudinal Acoustic mode), A_1- FLA (4/6), E_2-FTO (6/6)

(Folded Transversal Optical mode), E_2-type FTO (2/6) and E_1-type FTO (0) (unfolded mode, Γ point), respectively. [19] The E_1-type FTO (0) mode is forbidden in the backscattering (0001) geometry and its appearance in our spectra is connected with the stacking fault density [20]. In the damaged area of the ion implanted SiC, a peak at 960 cm^{-1} appears, corresponding to A_1-FLO (0). The assignment of the main Raman peaks of crystalline SiC is summarized in Table II.

The two intermediate spectra in Figure 2 present the strong modifications in the Raman spectra induced by the ion irradiation within the strongly modified regions for the low dose of Si ($4.17x10^{14}$ particles/cm^2) and the medium one of C ($2.02x10^{16}$ particles/cm^2). The top one is a characteristic spectrum from the heavily doped with Si ions (spot5, $9.17x10^{15}$ particles/cm^2). It is evident that the spectral area with the most significant changes from irradiation is between 430 to 1050 cm^{-1} with the appearance of strong bands, and this is the region where we focus our work. It is clear that almost two orders of magnitude less Si dose induces similar effects with C of the same energy. Furthermore, it is seen that in the high doping with Si ions spectrum there is no sign of crystalline peak and this is typical for the spectra close to the surface of the heavy dose spots (5 to 7). Concerning the wide bands, in Si irradiated samples we observe an increase of spectral yield around 930 cm^{-1}, while in the range 400-650 cm^{-1} the differences between the spectra from the two ions is minor. In the following we will concentrate mostly on the evolution of the E_2-FTO (2/6) crystalline peak, which is the only strong mode that is present in all C irradiated spectra, even from substantially damaged regions.

Typical modifications in the Raman spectra are presented in Fig. 3a, b for the lowest doses of C ($1.35x10^{15}$) and Si ($0.417x10^{15}$) ion implantation. For both the E_2-FTO peaks of crystalline SiC can be traced in all depths, strongly quenched in intensity but almost unshifted in energy. To the extent that the two peaks E_2-FTO (6/6) and E_1-type FTO (0) can be traced (Fig.3a), their relative intensity compared to E_2-FTO (2/6) is characteristic of the 6H-SiC structure [19]. This indicates that in spite of the strong lattice distortion, the basic structure remains unaltered by the ion irradiation in agreement with Bolse et al [14], who claim that the overall sp^3 bond structure is conserved, as well as the short-range order, where each Si atom is surrounded by four C atoms and vice versa. Because of the ion collisions, broad bands on either side of the crystalline peaks appear in the spectra from the damaged region, which are associated with lattice disorder introduced by the ion irradiation. Similar

broad bands have been detected by Raman spectroscopy in disordered SiC introduced by irradiation [4, 22-24]. The continuum on the left of the main peaks is composed of three bands; a broad one at ~535 cm^{-1}, characteristic of the Si-Si vibrations [25, 26] that could suggest a partial ordering of the Si-Si bonds in the SiC network, and two bands at ~600 and ~660 cm^{-1}, attributed to a slightly disordered structure [22]. The other continuum consists of two bands at ~870 and ~933 cm^{-1} attributed to amorphous or highly disordered SiC [22]. A peak at 966 cm^{-1} is visible in the second band, apparently corresponding to the A_1-FLO (0) mode [19], that should be present in our backscattering geometry, but it is probably activated by the breaking of the q≈0 selection rule in the damaged region. The assignment of the modes is summarized in Table 2 [19, 22].

The difference between the random (spot 7) and channeling (spot 6) irradiation with Si ions (same dose $4.17x10^{15}$ particles/cm^2) is presented in Fig.4, where in the inset the intensity of the main phonon peak at ~790 cm^{-1} is shown. As mentioned before, the damage with this high dose of Si atoms close to the surface is so strong that there is no trace of this main phonon peak, which gradually increases inside the compound, as shown in the inset. Concerning the broad bands, in the random mode there is a reduction in the spectral region ~930 cm^{-1}, which is similar to the one observed with high doses. Also, channeling appears to enter more inside than in the random irradiation (inset).

The analysis of the Raman spectra was carried out by fitting them with a mixture of Lorentz (crystalline peaks) and Gauss (broad bands) profiles as presented in Fig. 5 for the C ion implantation. Based on these fittings, we have calculated the dependence of the phonon characteristics on the doping level, the ion, and the depth. For the lowest doping with C (spot 4) and Si (spot 9) the results are presented in Fig.6, while similar results have been observed in all other cases. It occurs that for C the strong E_2-type FTO (2/6) phonon frequency shifts only slightly by ~0.6 cm^{-1} at a depth of ~2.8 μm from the surface. On the contrary, its intensity varies substantially, although close to the surface its variation also reproduces the loss of intensity from the leaking out of the beam due to its size. The phonon width is increased by ~21% (from 3.3 cm^{-1} to 4 cm^{-1}) at almost the same depth, indicating a lattice disorder. Similar to the irradiation of Si wafers [25, 26], this strong lattice disorder is attributed to the breaking of long range order [4, 22-24]. In Fig. 6a the size of the damaged stripe from SEM is indicated for comparison and it appears that the width of the

distorted region represents much better the damaged region, than the integrated intensity of the peak, while for the phonon frequency, no conclusion can be drawn due to the small shift. The depth dependence of the phonon width shows a steeper drop on the side closer to the front surface compared to the other side in close agreement with the SEM photo (Fig.1a). The shift in energy and the increase in the width of the main peak do not conform with a homogeneous disorder towards amorphization [27], but mostly to strained crystalline domains. As depicted in Fig. 3a, close to the surface (depth 0.4 μm) and deep inside (4.4 μm depth) the material is purely crystalline. At 2.8 μm the crystalline peaks have the lowest intensity and at 2.0 μm and 3.6 μm the situation is somewhere between. The broad bands do not seem to increase at the most damaged depth (2.8 μm), although the crystalline peak has been substantially quenched at this depth (Fig.3a). All these data show that the irradiation induces damage to the lattice leaving crystalline domains and amorphous regions randomly distributed inside the compound.

Similar results were observed with the low dose Si implantations (spots 8 and 9). In Fig. 6b, the selected E_2-type FTO (2/6) phonon shifts ~2 cm^{-1} at a depth ~2 μm from the surface. On the other hand, the phonon width is increased by ~30% (from 3.8 cm^{-1} to 5 cm^{-1}) at almost the same depth, indicating the modifications in the lattice. The integrated intensity of the peak plotted according to the depth in Fig.6b fails completely to reproduce the damaged zone as in the case of the C ions. The width of the damaged zone can be only roughly estimated from SEM (Fig.1b) because the boundaries are not well defined. Raman data represent very well this gradual change of disorder for both sides of the damaged zone.

Regarding the depth profile of the ion induced damage, the Raman results are in agreement with the SEM images, although the Raman transitions are gradual compared with the images that are sharp. The deviation is due to the size of the laser spot (~1 μm) that results in a convolution of spectra from different zones and accordingly in a more gradual transition between the zones. Concerning the two ions, we have observed that the C ions have reached deeper in the wafer and inflicted less damage, compared with the Si ions of the same energy, as expected from the difference in their atomic masses. Based on Monte Carlo calculations using SRIM-2013 for the 4 MeV C random implantation (bottom of Fig. 7) the ions reach a depth of 2.6 μm, while for the Si random implantation (top of Fig. 7) a depth 1.6 μm, both in good agreement with the SEM (Fig.1) and the width of the crystalline peak in the

Raman data (Figs. 6a and b). Furthermore, we have observed that the channeled ions reach deeper inside the SiC crystal than the randomly oriented ones (inset in Fig.4).

As presented in Fig.5, the continuum scattering in the spectra from damaged regions consists of wide bands, with the most prominent ones around ~533 cm^{-1} , ~870 cm^{-1} and ~933 cm^{-1}. In order to study the contribution of each wide band, Fig. 8 presents their relative intensities with respect to the crystalline E_2-FTO (2/6) peak for the C ions. The results for the low Si doses are similar, while for the higher ones, the crystalline peak is absent close to the surface. In Fig. 8 it is evident that the variation of the integrated intensity of the two broad bands discriminates well the damaged region. For the different doses of C the relative intensity of the broad bands compared with the crystalline peak, as well as the range of damage, increase with the amount of doping. Furthermore, the relative intensity of the two (left or right) continua remains roughly independent of the amount of doping and depth. It appears that for both C and Si implantations the lower energy broad band has a smaller contribution in the Raman spectra than the higher energy one for all doses used. Varying the dose roughly by a factor of three from the low dose of C, the Raman data show that there is no much difference in the geometrical distribution of damage in the system. But a further increase of dose induces more substantial modifications in the depth dependence of damage, indicating that the high dose has inflicted stronger distortions in the compound. It is possible there is a threshold in the number of ions introduced to the SiC, above which the evolution of the disorder is strongly modified, in agreement with previous conclusions [4, 22]. For the low doses, only a few ions can reach a depth greater than 2.8 μm, but as the ion fluence is increased, a greater number of channeled oriented ions could reach deeper, since the damaged zone transforms into an amorphous one, introducing Frenkel defects, antisite defects and interstitial clusters. Similar results are observed for the Si doses, suggesting that the type of ion that is introduced in the material, does not affect differently the 533 cm^{-1} band, which originates from Si vibrations. As a consequence, it is reasonable to assume that the intruding ions are not accommodated inside the SiC network to create bonds, but they rather displace mostly the C atoms. The increase of the dose above some level results in a destruction of the molecular bonds inside the SiC unit cell, leading to a completely distorted state. Based on that, one can assume that the “safe” doses of ion implantation that will induce lattice distortions anticipated by the Monte Carlo calculations is less than 6.74×10^{15} for C and 0.833×10^{15} for Si.

CONCLUSIONS

In conclusion, we have carried out a detailed study of the effect of 4 MeV C^{+3} and Si^{+3} ion irradiation of a 6H-SiC single crystal in the channeling mode by mapping the side cleaved profile of the damaged areas by micro-Raman spectroscopy and by comparison with the SEM pictures of the same regions. As expected, we have found that ions in the channeling mode travel more inside the crystal and C ions create well defined distorted domains parallel to the front surface, while Si ions destructions are shallower. It appears that the phonon bandwidth of the main SiC crystalline mode or the broad bands indicative of the lattice disorder map better the damaged regions and the results agree both with the SEM pictures and the Monte Carlo calculations. The evolution of the broad bands with ions and doses provided information about the lattice distortions inflicted by the ions showing a gradual destruction of the unit cell and formation of crystalline domains embedded in an amorphous surrounding.

ACKNOWLEDGEMENTS

MK and SP acknowledge partial support by the Horizon 2020 project AIDA-2020, GA No. 654168. SF acknowledges the support of the Croatian Science Foundation under the project MIOBICC (No. 8127).

Table I
Specimens studied

Spot	Irradiation particle	Fluence ($x10^{15}$ particles/cm^2)
1	Virgin	0
2	4 MeV C^{+3}	6.74
3	4 MeV C^{+3}	20.2
4	4 MeV C^{+3}	1.35
5	4 MeV Si^{+3}	9.17
6	4 MeV Si^{+3}	4.17
7	4 MeV Si^{+3} (random mode)	4.17
8	4 MeV Si^{+3}	0.833
9	4 MeV Si^{+3}	0.417

Table II
Peaks observed (cm^{-1})

Present work	Previous Work [19, 24]	origin	Attributed to :
149	150	Crystalline SiC	E_2-FTA (2/6)

240	241	Crystalline SiC	E_1-FTA (4/6)
265	266	Crystalline SiC	E_2-FTA (6/6)
507	504	Crystalline SiC	A_1-FLA (4/6)
515	514	Crystalline SiC	A_1-FLA (4/6)
~534	535	disorder	Si-Si vibrations
~600	600	disorder	Distorted/Disorder SiC
~661	660	disorder	Distorted/Disorder SiC
770	767	Crystalline SiC	E_2-FTO (6/6)
791	789	Crystalline SiC	E_2-FTO (2/6)
800	797	Crystalline SiC	E_1-FTO (0)
~866	870	disorder	Amorphous SiC
~930	933	disorder	Slightly disordered SiC
960	966	Crystalline SiC	A_1-FLO (0)

REFERENCES

1. Kokkoris, M., et al., *Determination of parameters for channeling of protons in SiC polytype crystals in the backscattering geometry.* Nuclear Instruments and Methods in Physics Research Section B: Beam Interactions with Materials and Atoms, 2001. **184**(3): p. 319-326.
2. Müller, G., G. Krötz, and E. Niemann, *SiC for sensors and high-temperature electronics.* Sensors and Actuators A: Physical, 1994. **43**(1-3): p. 259-268.
3. Sorieul, S., et al., *Raman spectroscopy study of heavy-ion-irradiated α-SiC.* Journal of Physics: Condensed Matter, 2006. **18**(22): p. 5235.
4. Chen, X., et al., *Irradiation effects in 6H–SiC induced by neutron and heavy ions: Raman spectroscopy and high-resolution XRD analysis.* Journal of Nuclear Materials, 2016. **478**: p. 215-221.
5. Kopsalis, I., et al., *Probing high-energy ion-implanted silicon by micro-Raman spectroscopy.* Journal of Raman Spectroscopy, 2014. **45**(8): p. 650-656.
6. Paneta, V., et al., *Investigation of deep implanted carbon and oxygen channeling profiles in [1 1 0] silicon, using d-NRA and SEM.* Nuclear Instruments and Methods in Physics Research Section B: Beam Interactions with Materials and Atoms, 2014. **320**: p. 6-11.
7. Kokkoris, M., et al., *Study of the irradiation damage in SiC by ion channeling.* Nuclear Instruments and Methods in Physics Research Section B: Beam Interactions with Materials and Atoms, 2002. **188**(1): p. 78-83.
8. Conrad, J., et al., *Irradiation effects in α-SiC studied via RBS-C, Raman-scattering and surface profiling.* Nuclear Instruments and Methods in Physics Research Section B: Beam Interactions with Materials and Atoms, 1996. **118**(1): p. 748-752.
9. Heera, V., et al., *Density and structural changes in SiC after amorphization and annealing.* Applied physics letters, 1997. **70**(26): p. 3531-3533.
10. Ohno, T., et al., *Electron microscopic study on residual defects of Al+ or B+ implanted 4H-SiC.* Journal of Electronic Materials, 1999. **28**(3): p. 180-185.
11. M., Erich, et al., *Micro-Raman depth profiling of silicon amorphization induced by high-energy ion channeling implantation.* Journal of Raman Spectroscopy, 2013. **44**(3): p. 496-500.

12. S. Nakashima, H. H., *Silicon Carbide – A Review of Fundamental Questions and Application to Current Device Technology*, W. J. Choyke, H. Matsunami , and G. Pensl, Editors. 1997, Akademie Verlag. p. 39.
13. McHargue, C. J., et al., *Damage accumulation in ceramics during ion implantation.* Nuclear Instruments and Methods in Physics Research Section B: Beam Interactions with Materials and Atoms, 1986. **16**(2): p. 212-220.
14. Bolse, W., et al., *Ion-beam-induced amorphization of 6H-SiC.* Surface and Coatings Technology, 1995. **74-75**: p. 927-931.
15. Pérez-Rodríguez, A., et al., *Analysis of Ion Beam Induced Damage and Amorphization of 6H-SiC by Raman Scattering*. JEM, 1996. **25**: p. 541-547.
16. Hobert, H., et al., *Infrared and Raman spectroscopy of particle-beam induced damage of silicon carbide.* Journal of Non-Crystalline Solids, 1997. **220**(2): p. 187-194.
17. Nakashima, S. and H. Harima, *Silicon Carbide : Recent Major Advances*, W.J. Choyke, H. Matsunami, and G. Pensl, Editors. 2004, Springer-Verlag Berlin Heidelberg. p. 585.
18. Harima, H., *Raman scattering characterization on SiC.* Microelectronic Engineering, 2006. **83**(1): p. 126-129.
19. Nakashima, S. and H. Harima, *Raman Investigation of SiC Polytypes*. Vol. 162. 1997. 39-64.
20. Wolfgang J. Choyke, H.M.a.G.P., ed. *Silicon Carbide : Recent Major Advances*. 1 ed. Advanced Texts in Physics. 2004, Springer-Verlag Berlin Heidelberg. XXXIV, 899.
21. Motooka, T. and O. W. Holland, *Amorphization processes in ion implanted Si: Ion species effects.* Applied Physics Letters, 1992. **61**(25): p. 3005-3007.
22. Chaabane, N., et al., *Investigation of irradiation effects induced by self-ion in 6H-SiC combining RBS/C, Raman and XRD.* Nuclear Instruments and Methods in Physics Research Section B: Beam Interactions with Materials and Atoms, 2012. **286**: p. 108-113.
23. Linez, F., et al., *Determination of the disorder profile in an ion-implanted silicon carbide single crystal by Raman spectroscopy.* Journal of Raman Spectroscopy, 2012. **43**(7): p. 939-944.
24. Koyanagi, T., Lance, M. J., and Katoh, Y., *Quantification of irradiation defects in beta-silicon carbide using Raman spectroscopy*. Scripta Materialia, 2016. **125**: p. 58-62.
25. Zwick, A. and R. Carles, *Multiple-order Raman scattering in crystalline and amorphous silicon.* Physical Review B, 1993. **48**(9): p. 6024.
26. Lannin, J., et al., *Variable structural order in amorphous silicon.* Physical Review B, 1982. **26**(6): p. 3506.
27. Nakashima, S., et al, *Phonon Raman scttaering in disordered silicon carbides*. Phil. Mag. B, 1994. **70**: p. 971-985.

FIGURE CAPTIONS

Figure 1. SEM profile of (a) the C (spot 4) implantation and (b) that of Si (spot 9).

Figure 2. Raman spectra from virgin (non-irradiated) SiC (bottom spectrum), from C irradiation (spot 3, 2.8 μm inside the material) and from Si (spot 9, 1.2 μm inside).

Inset: estimate of the laser spot diameter. Inset: E_2-FTO (2/6) intensity variation by scanning across the surface of virgin SiC (data points), best fit using Boltzmann function (red in colour), and derivative of best fit (blue in colour).

Figure 3. Evolution of the micro-Raman spectra by scanning across the side cleaved surface of implanted spots (a) with C ions (1.35×10^{15} particles/cm^2) and (b) Si ions (0.417×10^{15} particles/cm^2).

Figure 4. Comparison of strongly distorted regions in channeling and random mode Si irradiation with 4.17×10^{15} particles/cm^2. Inset: variation of the strong crystalline peak (~790 cm^{-1}) intensity inside the crystal in random and channeling mode.

Figure 5. Fit of the 1st and 2nd order bands with Lorentzian and Gaussian shapes.

Figure 6. Variation of the phonon peak position (crosses –blue in colour- left scale, bottom graph), integrated intensity (diamonds –red in colour- right scale, bottom graph), and FWHM (black triangles, upper graph) of the (a) C (spot 4) and (b) Si (spot 9) implantation.

Figure 7. Comparison of variation of the FWHM of the strong crystalline peak (~790 cm^{-1}) with results of Monte Carlo simulation of the collision events inside the compound from C (bottom) and Si (top) ion implantations.

Figure 8. Relative amount of the ~533 cm^{-1} band intensity (bottom graph) or of the sum of the bands at ~870 cm^{-1} and ~933 cm^{-1} area (top graph) to the E_2-FTO (2/6) crystalline peak at 790 cm^{-1}, for all three doses of C irradiation.

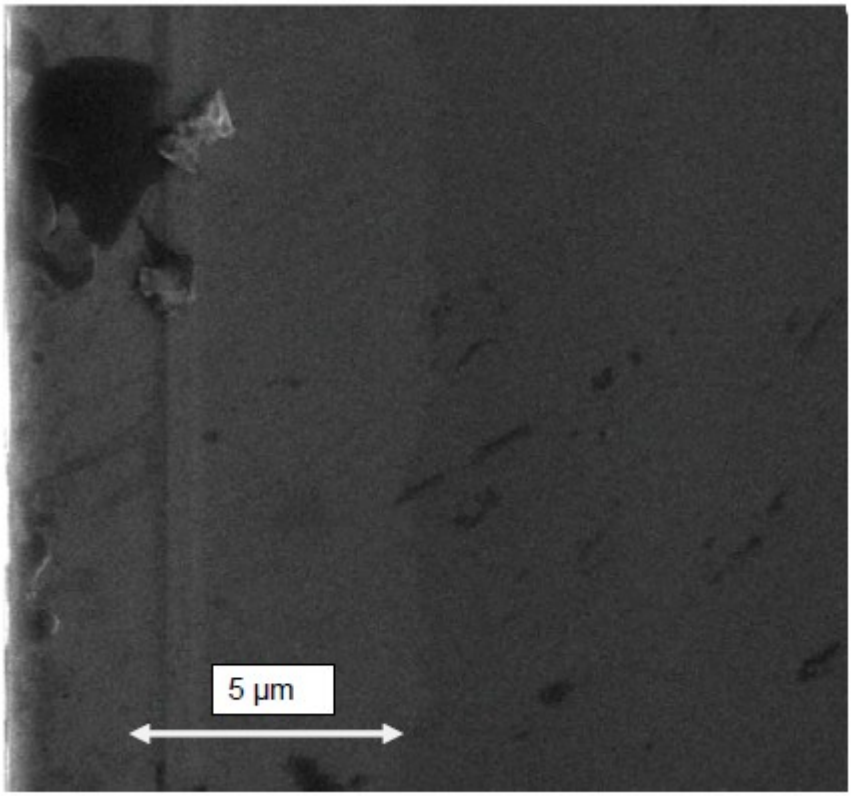

Fig. 1a

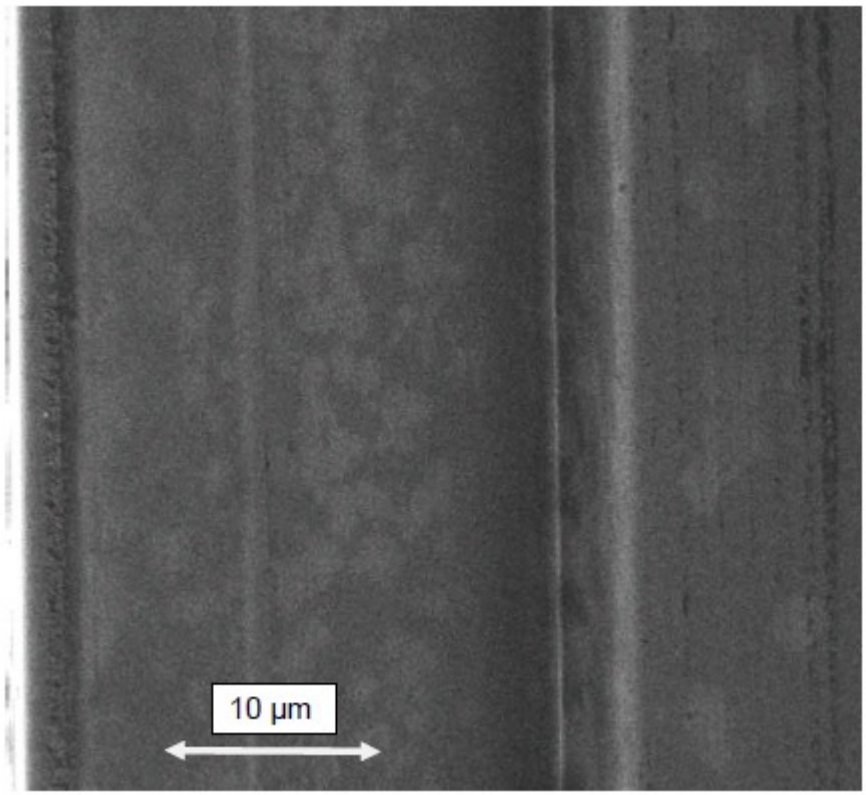

Fig. 1b

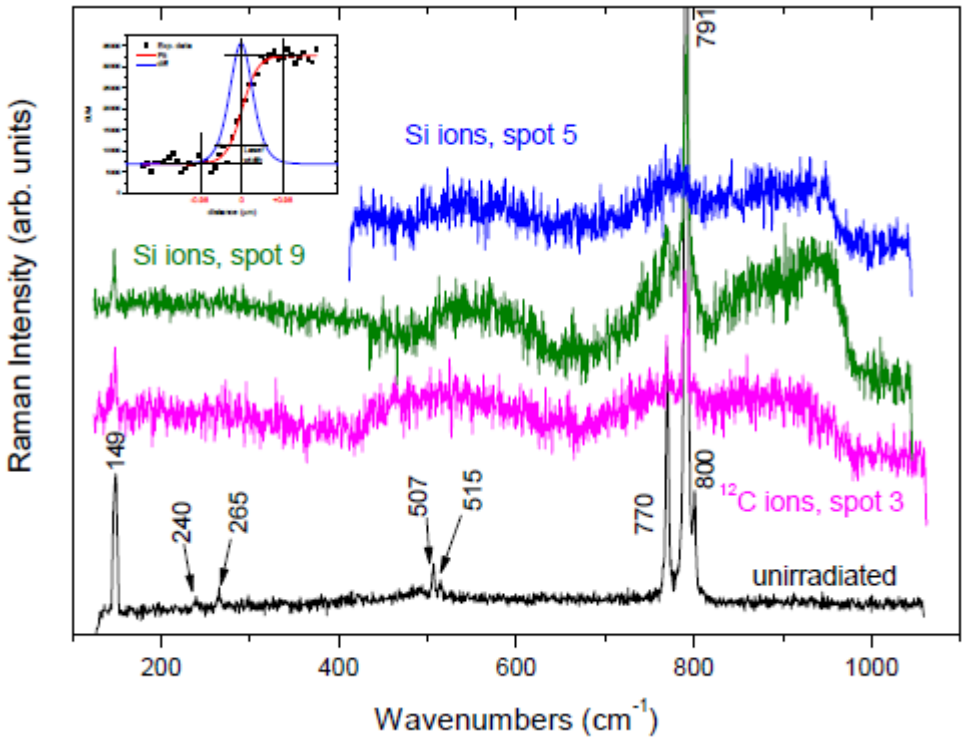
Raman Intensity (arb. units)
Wavenumbers (cm-1)
200
400
600
800
1000
Si ions, spot 5
Si ions, spot 9
12C ions, spot 3
unirradiated
149
240
265
507
515
770
791
800

Fig. 2

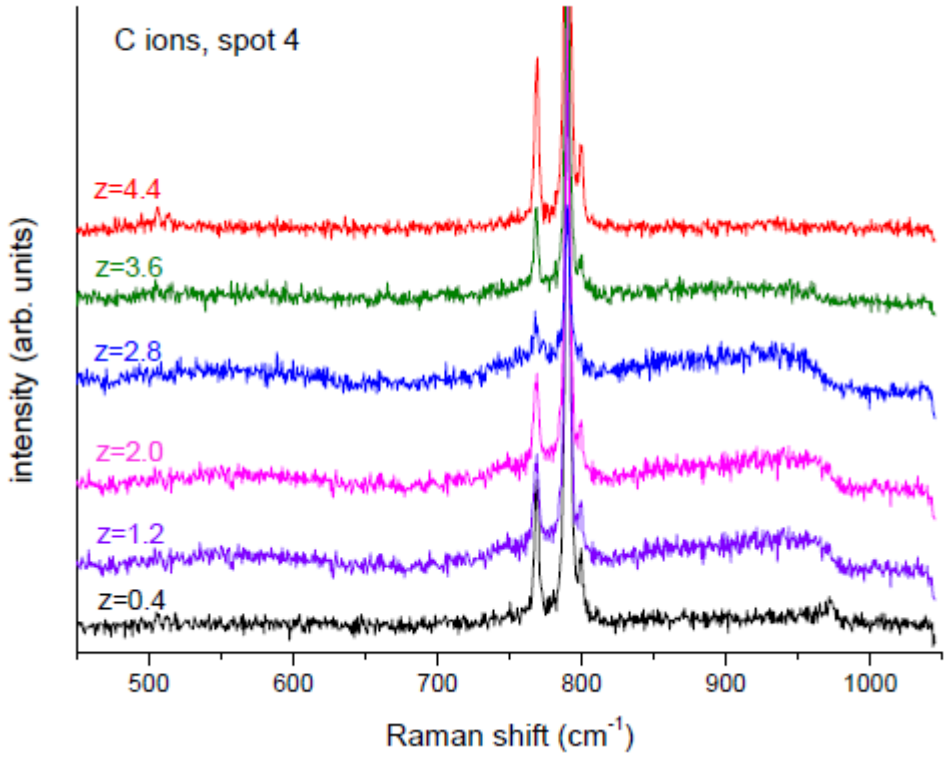
C ions, spot 4
z=4.4
z=3.6
z=2.8
z=2.0
z=1.2
z=0.4
intensity (arb. units)
500
600
700
800
900
1000
Raman shift (cm-1)

Fig. 3a

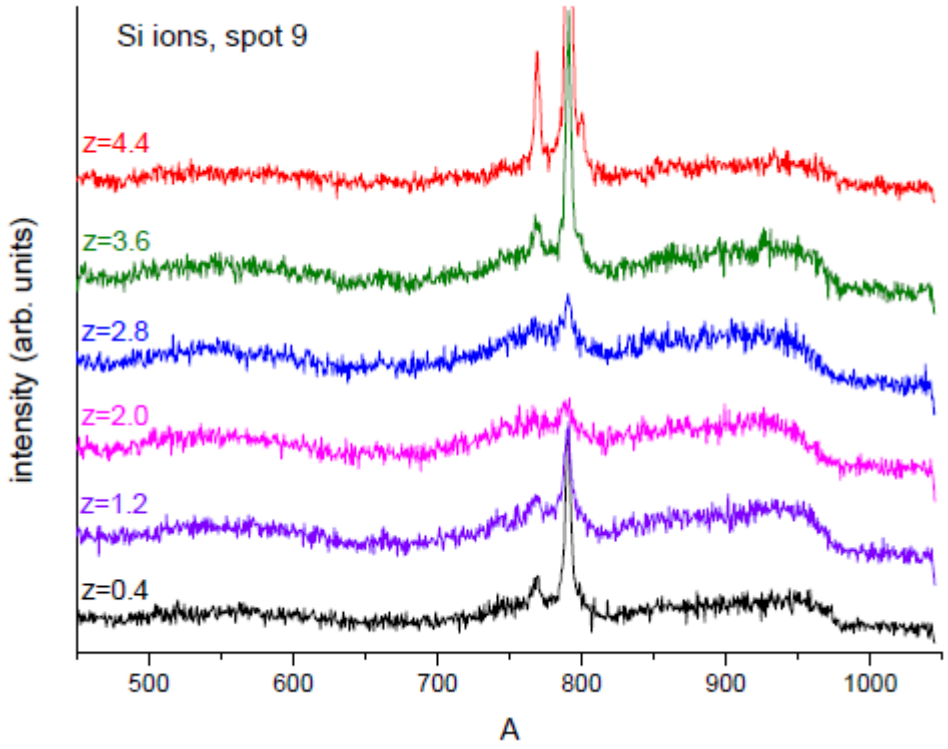
Si ions, spot 9
z=4.4
z=3.6
z=2.8
z=2.0
z=1.2
z=0.4
intensity (arb. units)
500
600
700
800
900
1000
A

Fig. 3b

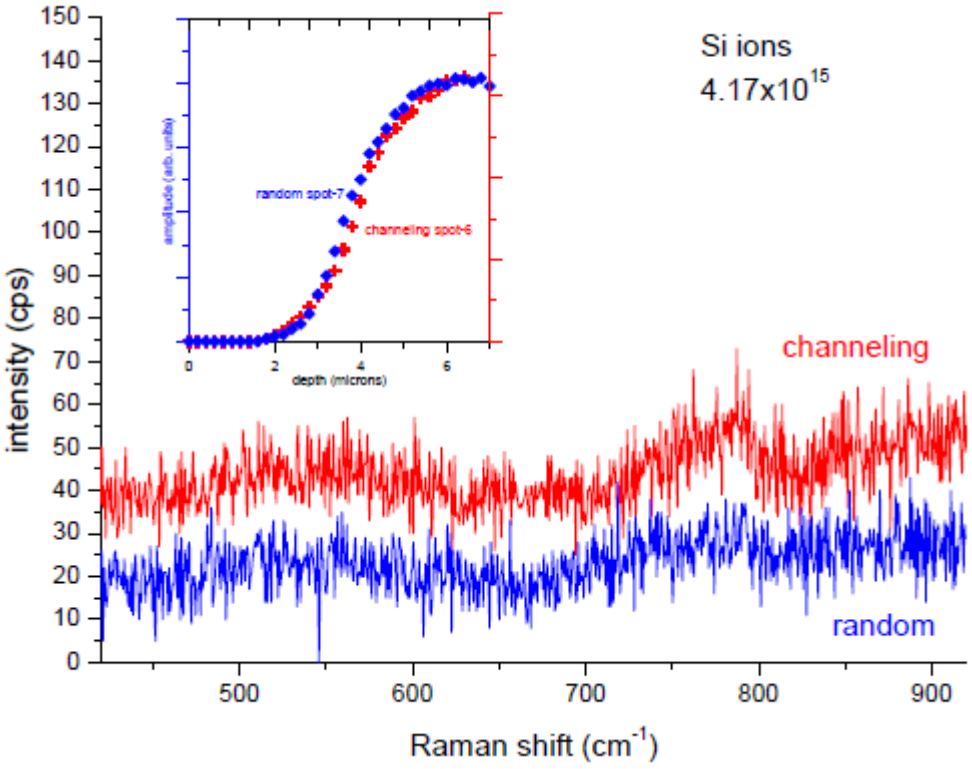
Si ions
4.17x10^15
channeling
random
intensity (cps)
Raman shift (cm^-1)
random spot-7
channeling spot-6
depth (microns)
amplitude (arb. units)

Fig. 4

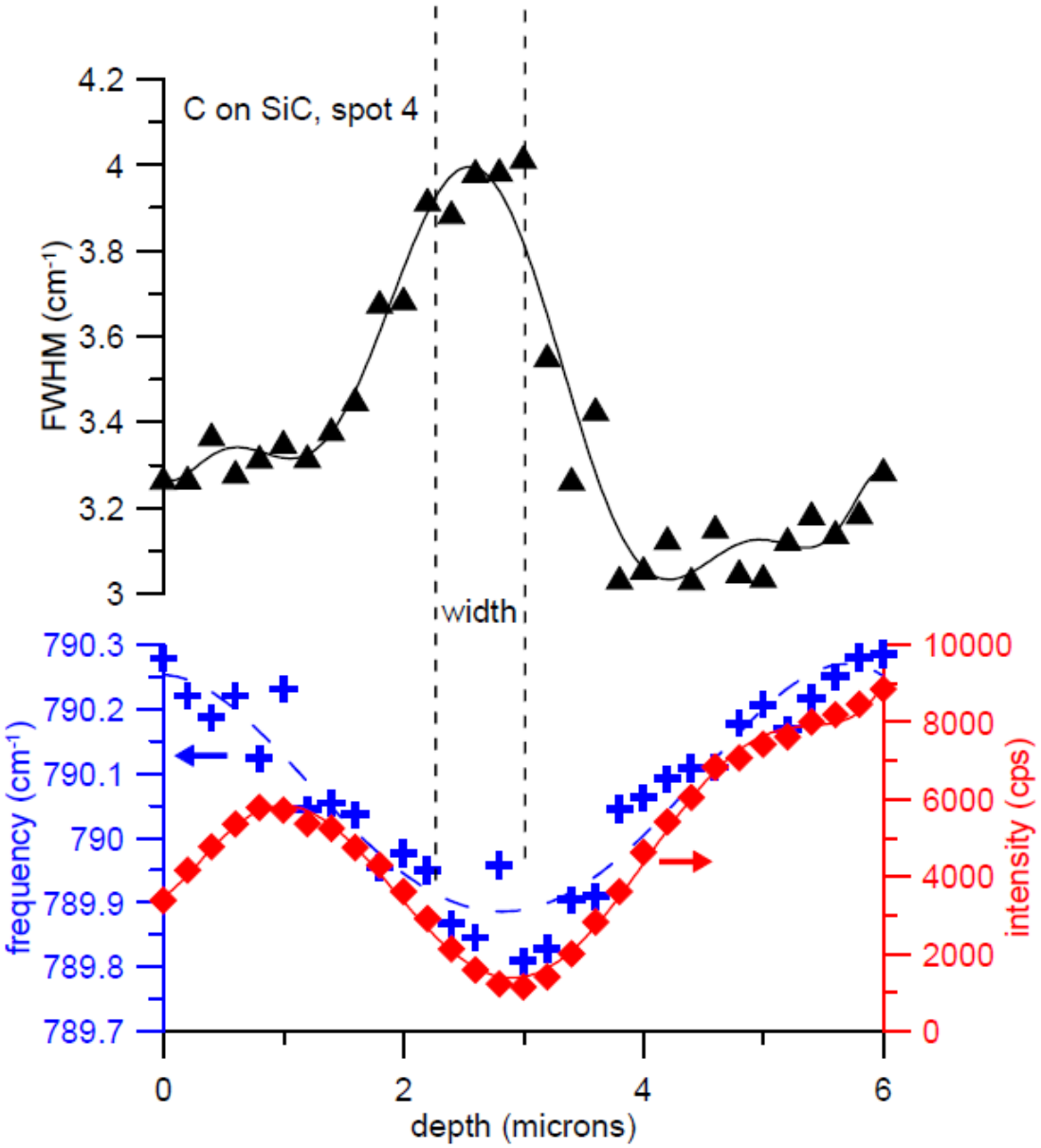
C on SiC, spot 4
FWHM (cm-1)
4.2
4
3.8
3.6
3.4
3.2
3
width
790.3
790.2
790.1
790
789.9
789.8
789.7
frequency (cm-1)
10000
8000
6000
4000
2000
0
intensity (cps)
0
2
4
6
depth (microns)

Fig. 6a

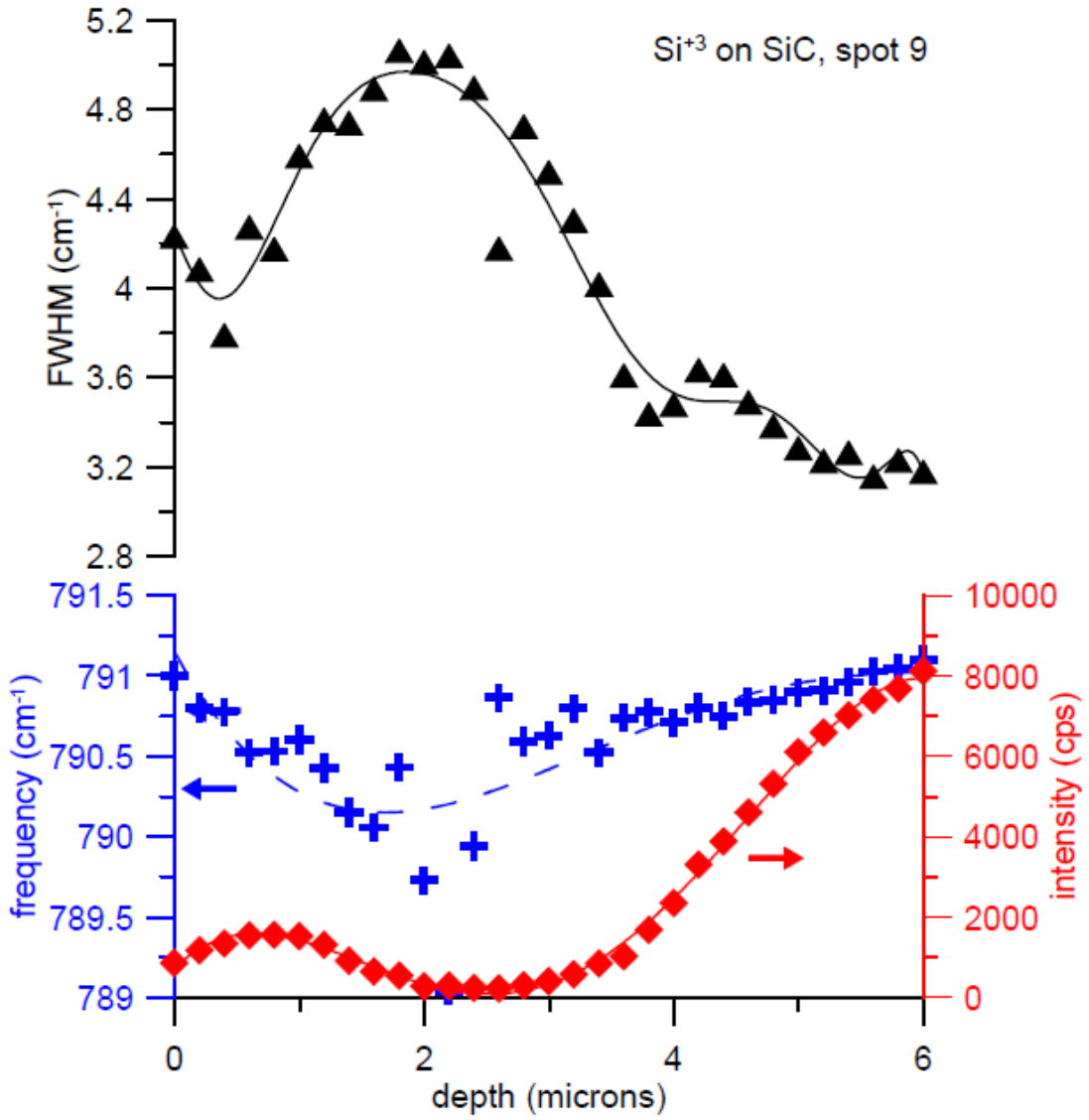
Si+3 on SiC, spot 9
FWHM (cm-1)
5.2
4.8
4.4
4
3.6
3.2
2.8
frequency (cm-1)
791.5
791
790.5
790
789.5
789
intensity (cps)
10000
8000
6000
4000
2000
0
0
2
4
6
depth (microns)

Fig. 6b

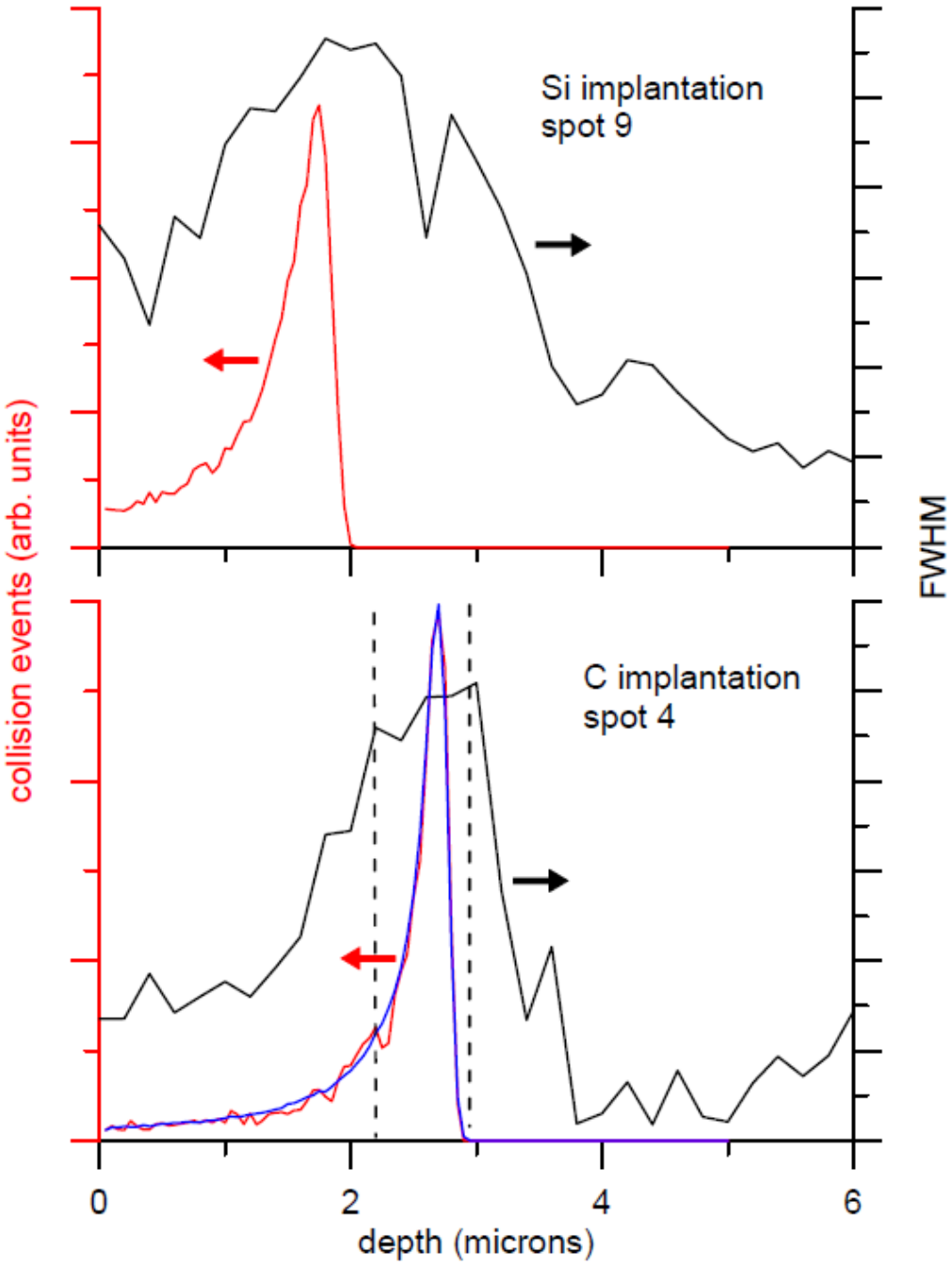
Si implantation
spot 9
C implantation
spot 4
collision events (arb. units)
FWHM
0
2
4
6
depth (microns)

Fig. 7

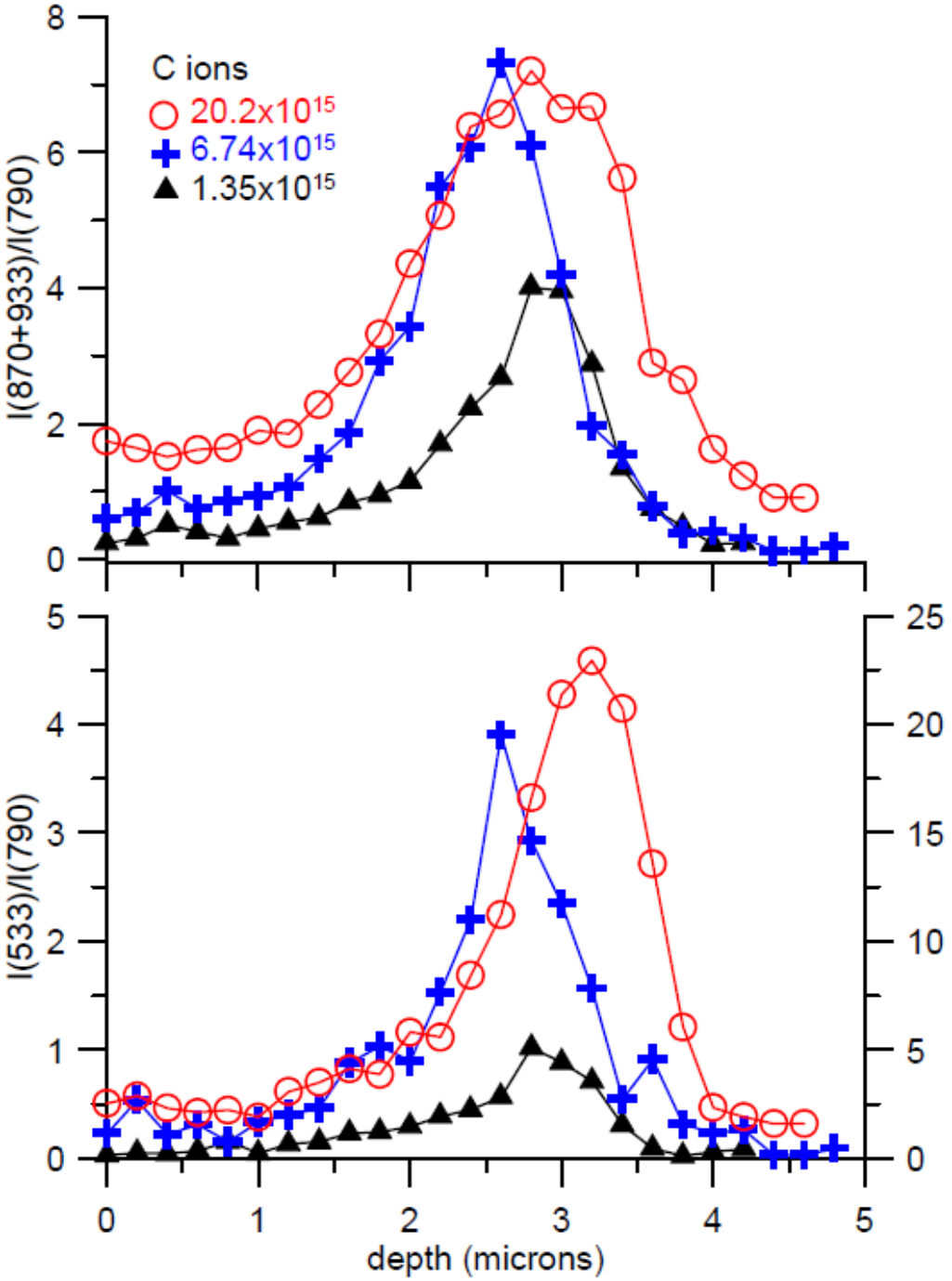
C ions
20.2x10^15
6.74x10^15
1.35x10^15
I(870+933)/I(790)
I(533)/I(790)
depth (microns)
0
1
2
3
4
5
0
2
4
6
8
0
1
2
3
4
5
0
5
10
15
20
25

Fig. 8